

TKT4142 Finite Element Methods in Structural Engineering

CASE STUDY 6

SOLUTION PROPOSAL

Case Study 6 use a thin-walled canal cross-section to address the modelling of shell problems (i.e., $h/L < 1/10$). The purpose is to provide knowledge and experience in how to use shell elements to model thin-walled beam sections. We will also compare the solution obtained with various type of shell elements to that using beam elements and/or beam theory. A workshop on how to model the different aspects addressed in this case study is uploaded to Blackboard (see “Workshop6.pdf” in the folder “Case studies”).

Learning outcome:

- Modelling of plate problems
- Convergence studies
- Knowledge and experience in modelling thin-walled beam sections with various shell and beam element types

Problem description

Figure 1 shows a cantilevered beam with a thin-walled canal cross-section. The beam is fixed on one end and a line load is applied to the top flange on the other end. The beam should be modelled and analysed with ABAQUS. The material properties correspond to structural steel.

Shell model

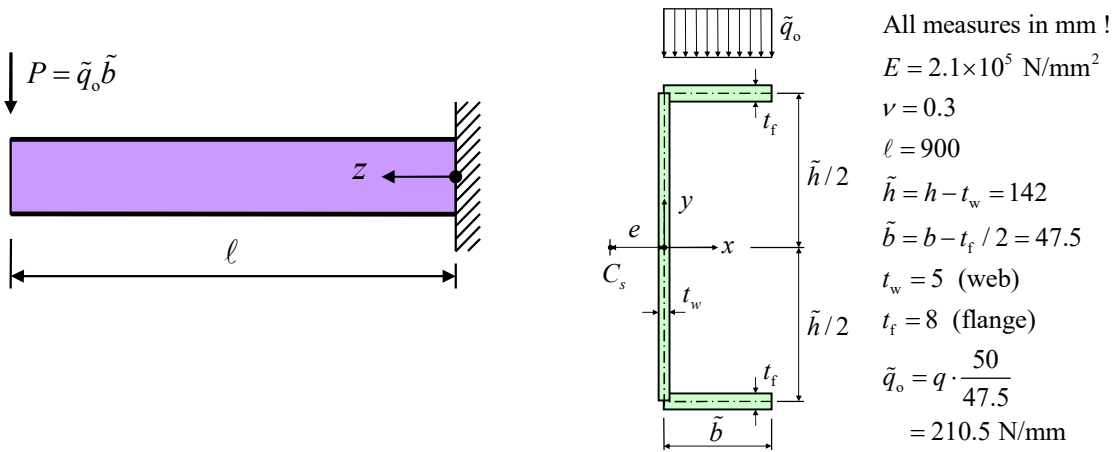


Figure 1: Cantilever beam fixed in one end and loaded with a line load to the top flange in the other end.
 All measures are in millimeters.

Load: $q_0 = -200 \text{ N/mm}$ (downwards)

Material data: $E = 210\,000 \text{ N/mm}^2$, $\nu = 0.30$, $l = 900 \text{ mm}$, $\sigma_y = 355 \text{ N/mm}^2$

A note on the element types and meshes:

To investigate the effect of the discretization (both number of elements and form) and the polynomial order it has been conducted simulations on 6 different regular meshes with 5 different element types both linear and quadratic. Table 1 gives the six different meshes in terms of number of elements in length, width and height direction, n_ℓ , n_b and n_h respectively, and total number of elements, N_{els}^Δ and N_{els}^\square , when triangular and rectangular elements are used. Note that the number of elements in the width direction (n_b) does not double between mesh B and C, and C and D. The reason being that it is preferable to keep the ratio between the lengths of the element sides as close to one as possible, in addition there are only small gradients in the stress field over the width of the flange. Figure 2 shows mesh A and B with rectangular and triangular elements respectively.

Number	Mesh					
	A	B	C	D	E	F
n_ℓ	12	24	48	96	192	384
n_b	1	2	3	5	10	20
n_h	2	4	8	16	32	64
N_{els}^Δ	96	384	1344	4992	19968	79872
N_{els}^\square	48	192	672	2496	9984	39936

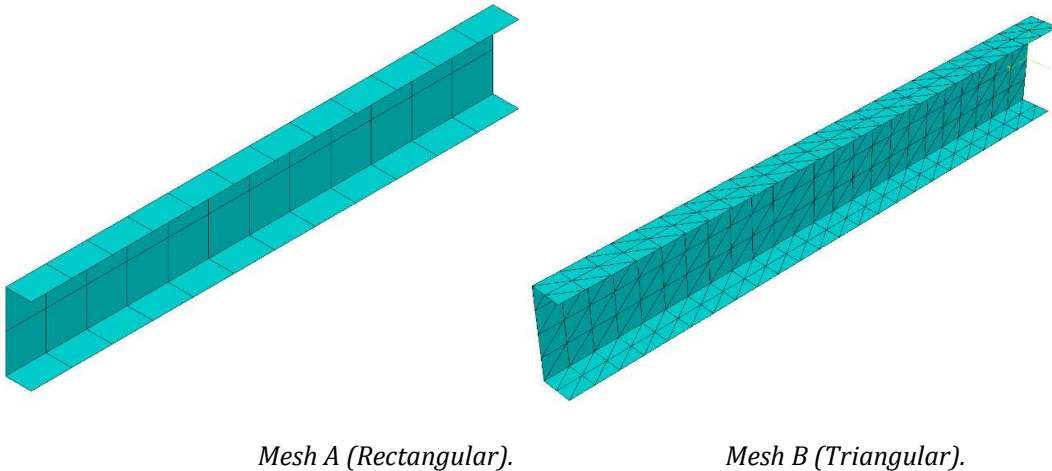
Table 1: Mesh and number of elements.

Mesh A-E is analyzed using both linear and quadratic triangular and rectangular elements, while Mesh F is only analyzed using linear triangular and quadratic elements. The following elements have been used:

- S3: 3-node linear triangular shell element for large deformations
- STRI3: 3-node linear triangular thin shell element for small deformations
- STRI65: 6-node quadratic triangular thin shell element
- S4: 4-node bi-linear rectangular shell element with full integration
- S8R: 8-node quadratic rectangular thick shell element with reduced integration

S3 and S4 elements could be used on both thin and thick shells, while the rest of the elements are specifically designed for either thick or thin shells. The membrane part of the S4 element is based on assumed strains (ANS = Assumed Natural Strains), which yields an element that is more robust and has higher accuracy when the element is irregularly shaped compared to a displacement-based element. In all of our meshes the elements are rectangular shaped such that we don't benefit from the fact that S4 is more robust. The accuracy of the membrane part of S4 is similar to a QM6 element and significantly better than a fully integrated or selectively reduced integrated Q4 element.

The problem we are going to analyze is dominated by bending, where the forces are primarily carried by membrane forces in the web. Bending will be present in the flanges but would not influence the global solution significantly. Thus, using elements that are designed for thin or thick shells is rather insignificant for the study performed in this exercise.



Mesh A (Rectangular).

Mesh B (Triangular).

Figure 2: Meshes.

Task a) Perform a convergence study and compare the largest bending stresses and displacements based on finite element analysis of both linear and quadratic, triangular and square shell elements. Explain how the convergence study has been conducted.

Solution:

Note: This solution proposal is quite extensive and covers a wide range of both element types and element sizes. This is to highlight the differences in convergence and performance.

Convergence study with shell elements

Figures 3 and 4 show the convergence plots of respectively vertical and horizontal displacement of the free end of all 28 combinations of elements and element network that is analyzed. Vertical displacement is registered at the middle of the web, while horizontal displacement is registered at the top of the web. We observe that the triangular elements STRI65 and S3 converges slower than the other three elements STRI3, S4 and S8R. Convergence plots also show that STRI3 converge towards significantly lower values than the other elements, while triangular elements S3 and STRI65 converge towards higher values than square elements S4 and S8R. Element S4 look otherwise appear to converge to a value of 4.82 and 9.30 mm for vertical and horizontal displacement of the free end. The results show that horizontal displacement at the top of the web is as great and opposite as the horizontal displacement of the bottom of the web and can therefore be used as a measure of the twist (rotation about the longitudinal axis) for that cross-section.

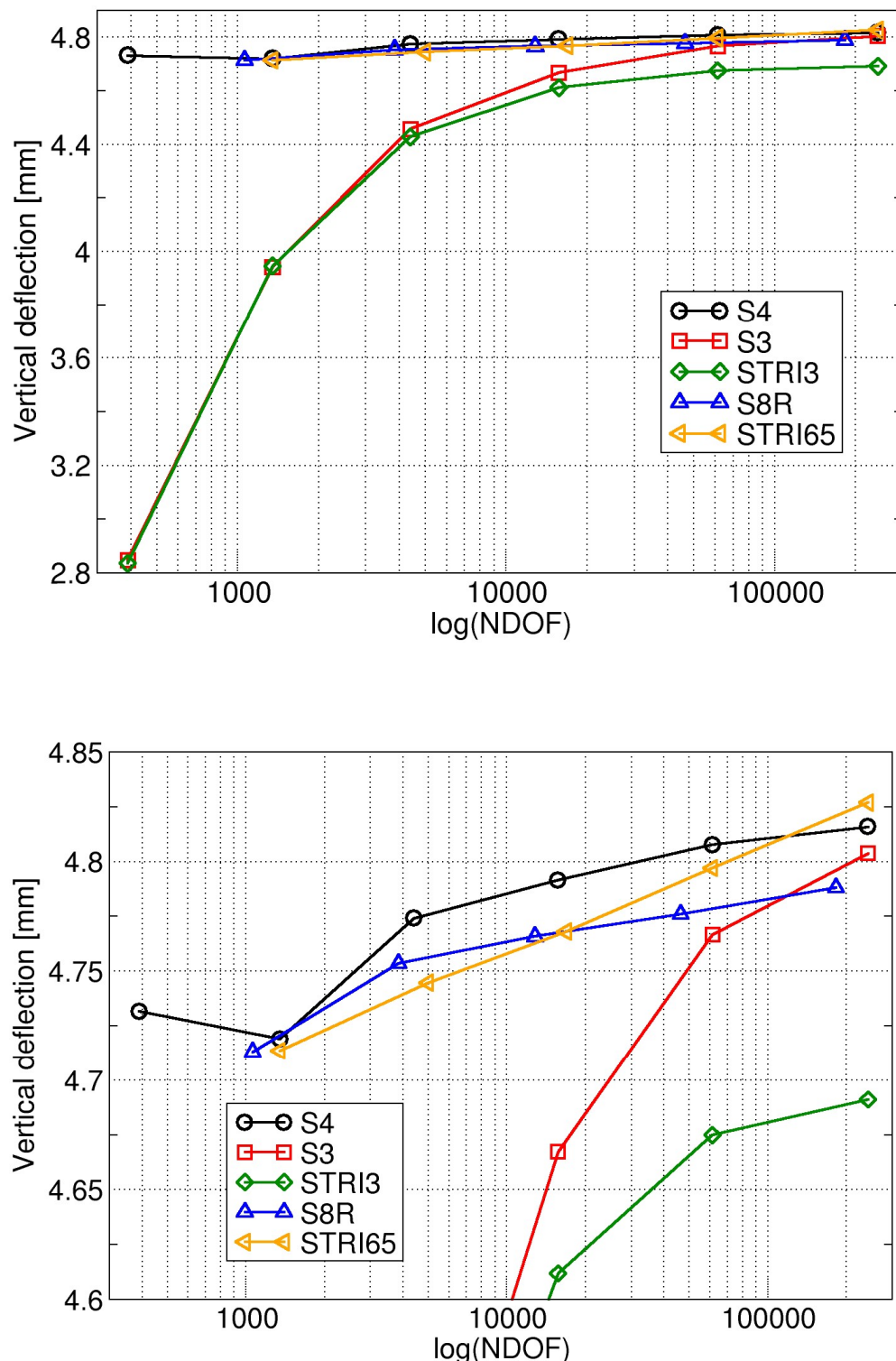


Figure 3: Convergence plot of vertical deflection of free end.

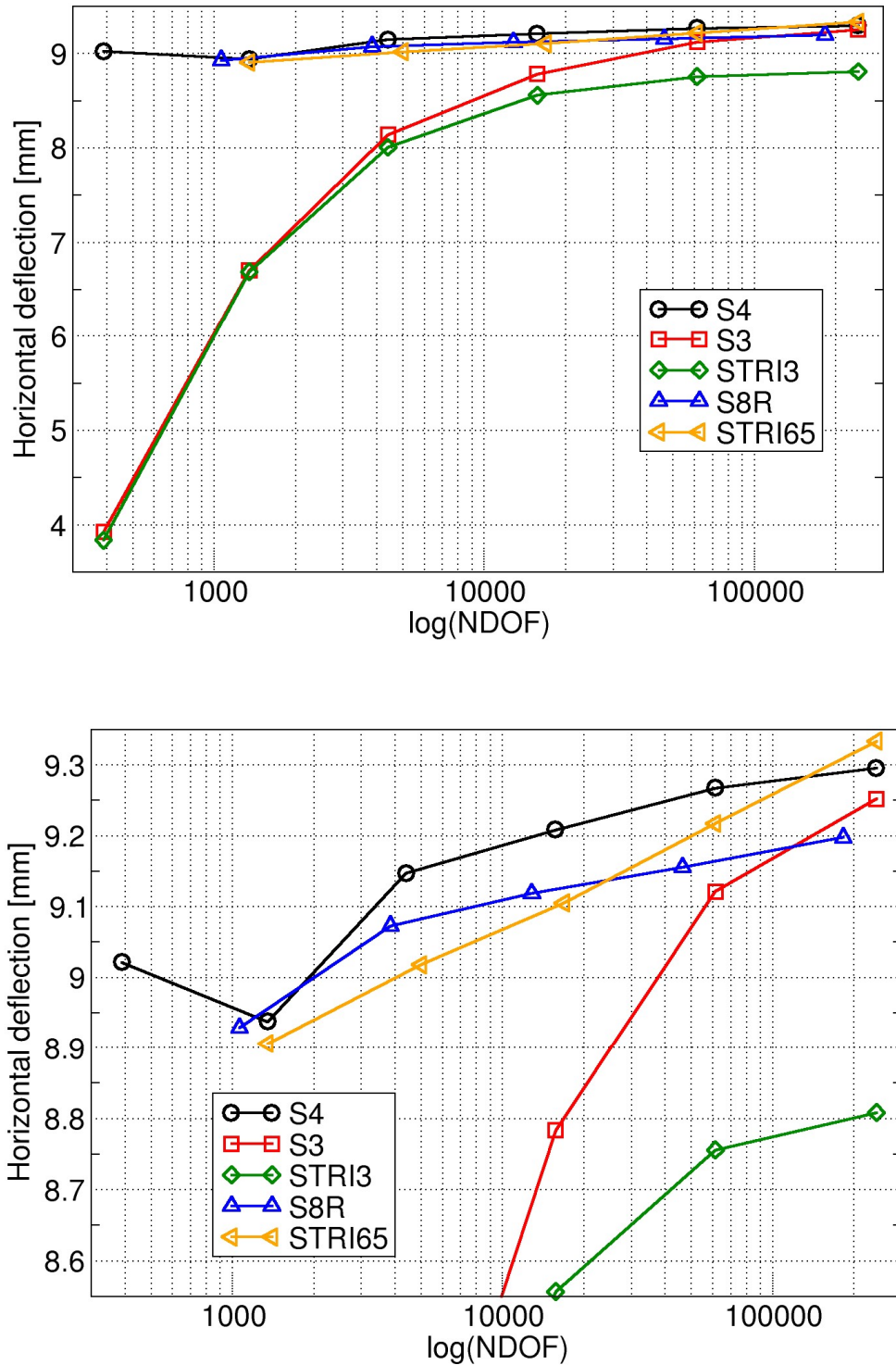


Figure 4: Convergence plot of horizontal displacement of free end.

Figure 5 shows the corresponding convergence plot of the maximum bending stress at the fixed end. None of the elements converge, due to stress concentrations arising in the top and bottom of the cross-section at the fixed end. As we decrease the size of the elements $h \rightarrow 0$ the stresses will $\sigma \rightarrow \infty$. To avoid stress concentrations at the fixed end, it may be appropriate to look at a section that is not affected by these local effects.

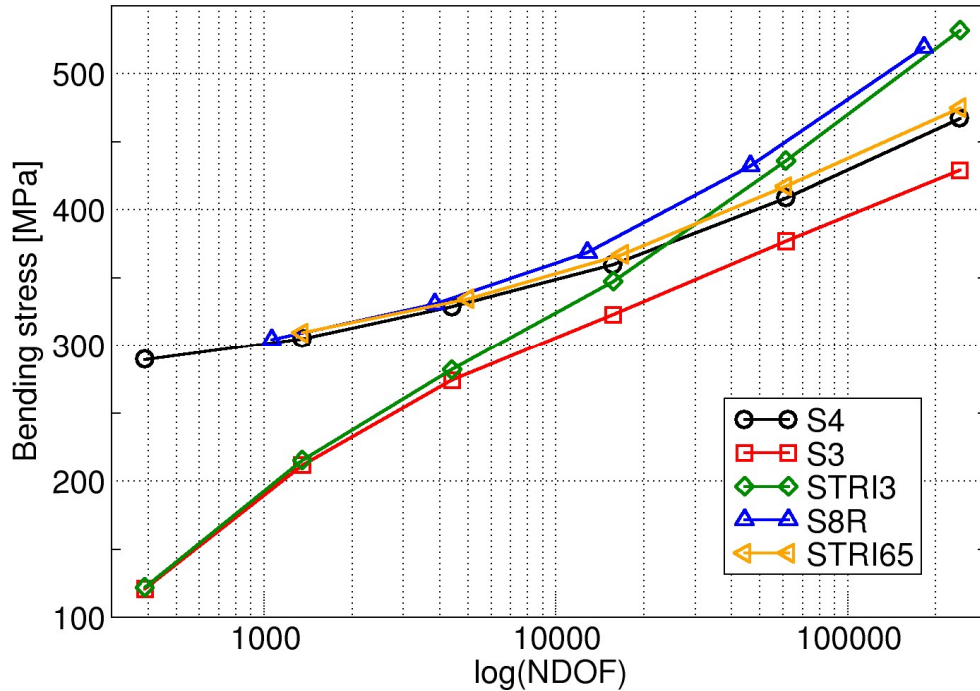


Figure 5: Convergence plot of maximum bending stress at the fixed end.

Figure 6 shows the convergence plot of the maximum bending stress of $z = \ell/2 = 450$ mm, which corresponds to the beam center section. Membrane part of S3 and STRI3 cannot describe a linear variation of strains/stresses within the element (cf. the characteristics of CST element subjected to plane bending). This explains why the results obtained with linear triangular element converges more slowly than the other elements. Similar to what was observed in convergence plotted for displacements in Figures 3 and 4, triangle elements STRI65 and S3 converge slower than the other three elements STRI3, S4 and S8R. Similarly, we observe also that STRI3 converges towards lower values than the other elements, while triangular elements S3 and STRI65 converge towards higher values than square elements S4 and S8R. Element S4 converges towards a value of 125 MPa.

It is also important to note that stresses presented in Figures 5 and 6 do not represent actual element solution σ^h , but a post-processed smoothed stress field, σ^* , based on “nodal averaging”. Note that if the difference in the FE solution σ^h between two neighboring elements is too large for the user-defined limit, which in ABAQUS is set to 75 %, the stresses will not be smoothed. This limit could be changed, and by specifying it equal to 0 %, the solution will not be smoothed at all. If it is put equal to 100 % the average value is calculated regardless of the discontinuity between the elements. It is not recommended to put it higher than 75 %, as it would make it difficult to spot discretization errors that are caused by too coarse mesh or too

low polynomial order. Large discontinuities also characterize areas with irregular element shape.

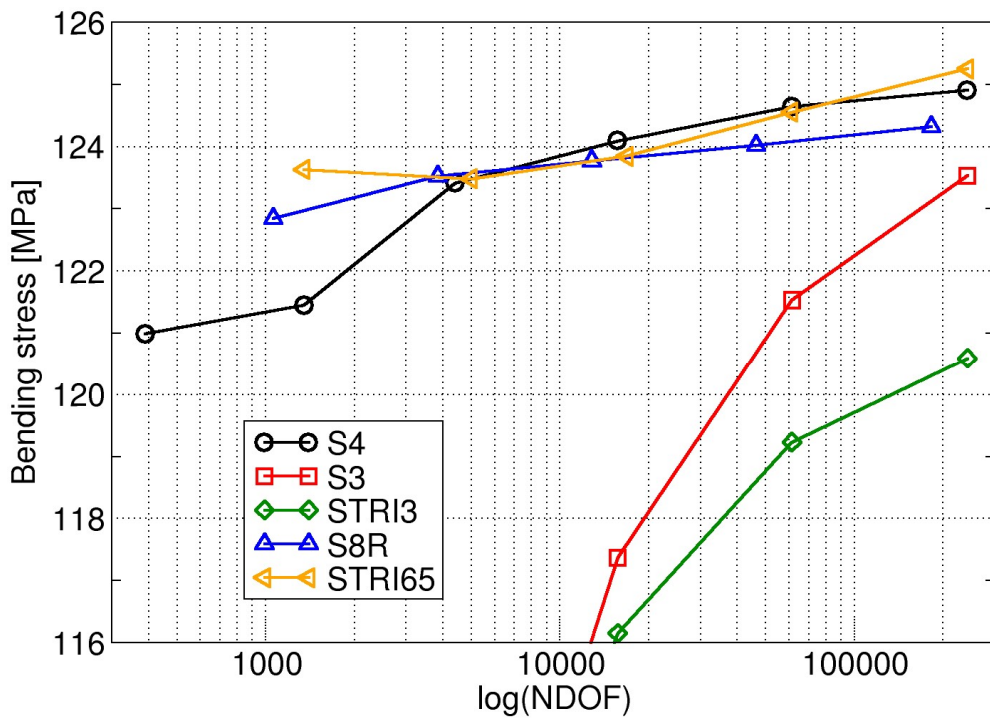
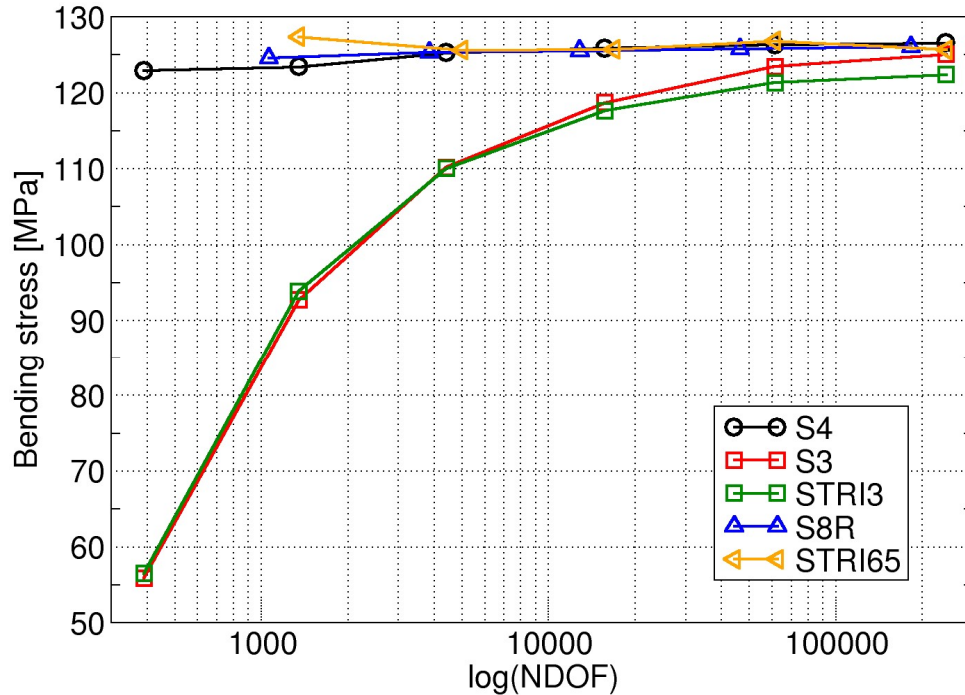
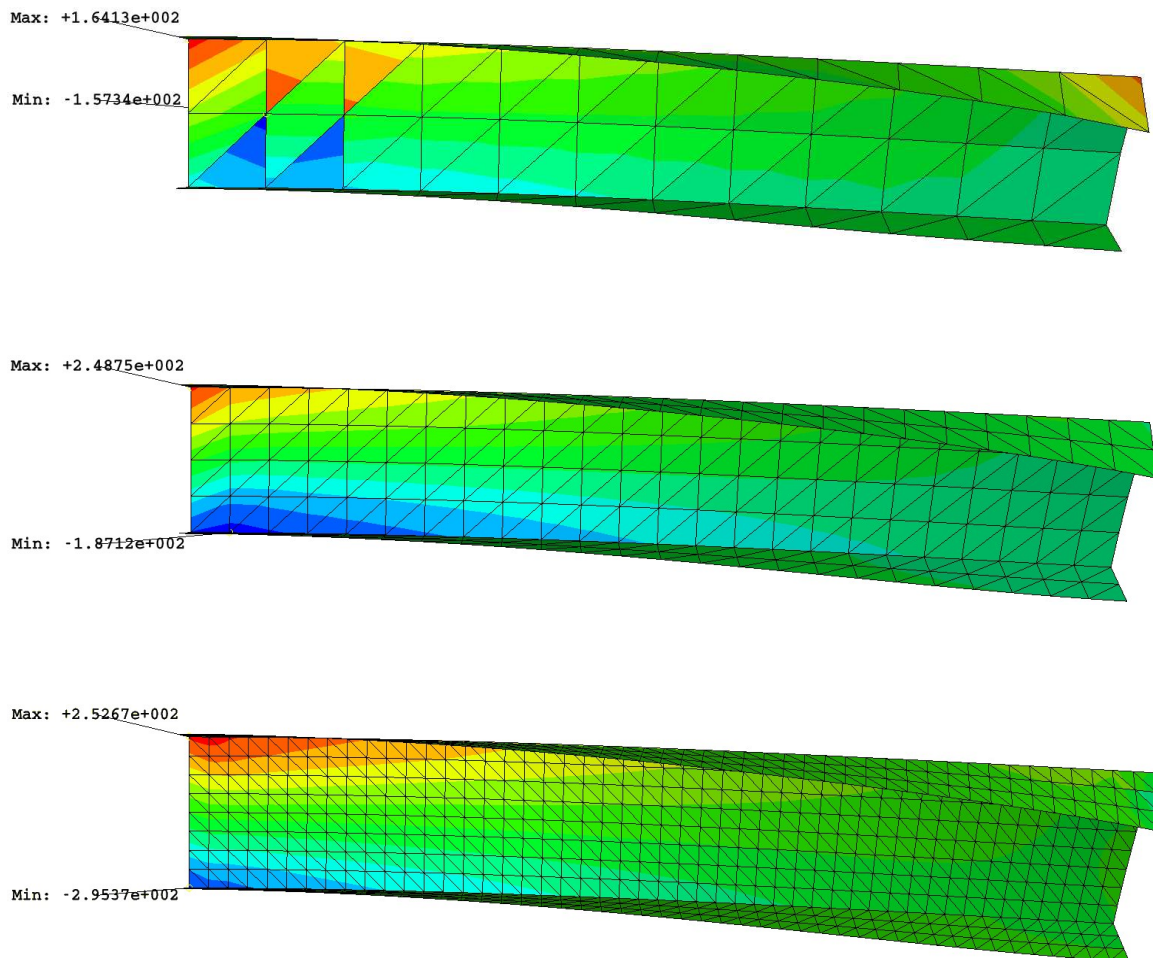


Figure 6: Convergence plot of maximum bending stress in the middle of the beam.

Figure 7 shows how the stresses are varying over the whole model, in terms of a contour plot of the bending stresses on the deformed geometry, for element S3, Mesh A-E. For the coarsest mesh, Mesh A, we see several examples of the bending stresses σ^h not being smoothed between the elements. This is caused by, as mentioned above, that the requirement of maximum 75 % difference between the elements is not satisfied.

From Figure 7 we observe that the bending stress distribution for triangular elements is not symmetrical over the height of the cross-section. This is because the meshes are not symmetrical, which means that the stresses in the upper and lower edge of the cross-section in the fixed end which are opposite equal for the square elements, do not have the same amplitude for analyzes with triangular elements. Convergence plots with maximum bending stress for triangular elements thus indicates the average of the amplitudes of bending stress appearing in the top and bottom edges of the cross-section.



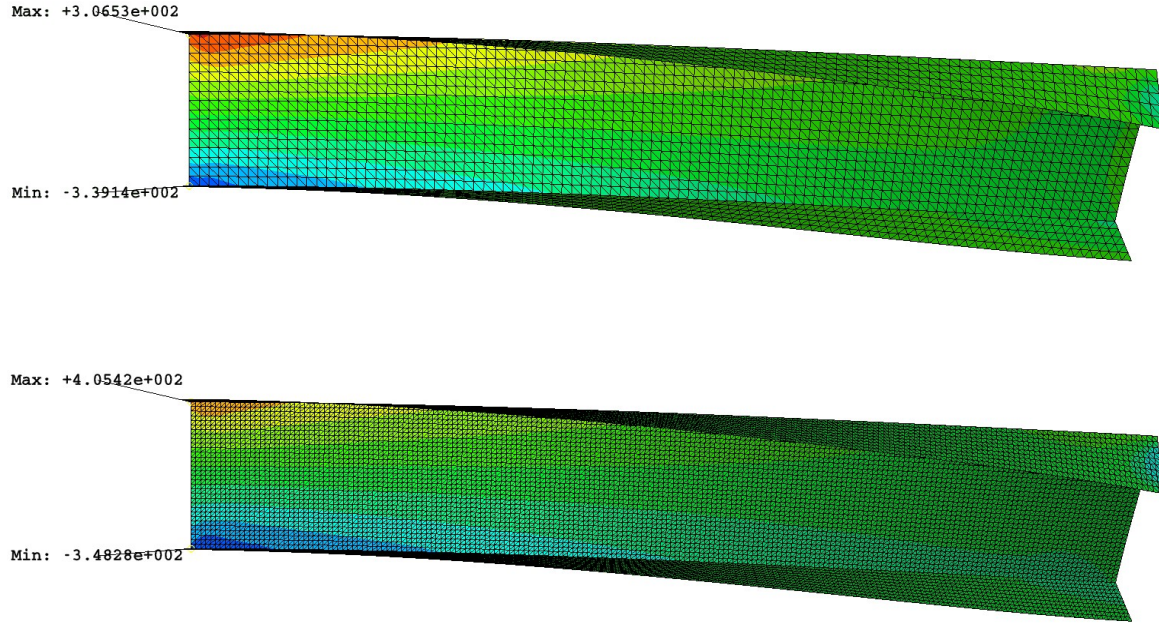


Figure 7: Contour plot of bending stresses for element S3 for mesh A-E.

Figure 8 shows the stress distribution over the web for element S4, Mesh A-F, for the beam end and middle respectively ($z = 0$ and $z = \ell/2$ in Figure 1). As mentioned above, it is clear that as the mesh is refined, $h \rightarrow 0$, the stresses $\sigma \rightarrow \infty$ at the top and bottom of the cross-section at the fixed end ($z = 0$). We also observe an approximately linear variation of the bending stresses over the height for all meshes (Mesh A-F) in the middle of the beam ($z = \ell/2$).

Finally, it should be mentioned that the stresses in the shell elements are reported at the bottom surface, unless otherwise specified. To ensure that plots show extremal values regardless of which surface (upper or lower edge) they are referred to, it is recommended to use the following menu options:

Results → Field Output

Click the button “**Section Points**” in the window “**Field Output**” to bring up the dialog box to select which sample points to be used for visualization of results. In the dialog box “**Section Points**” it is recommended to use the setting:

Active locations → Top and bottom

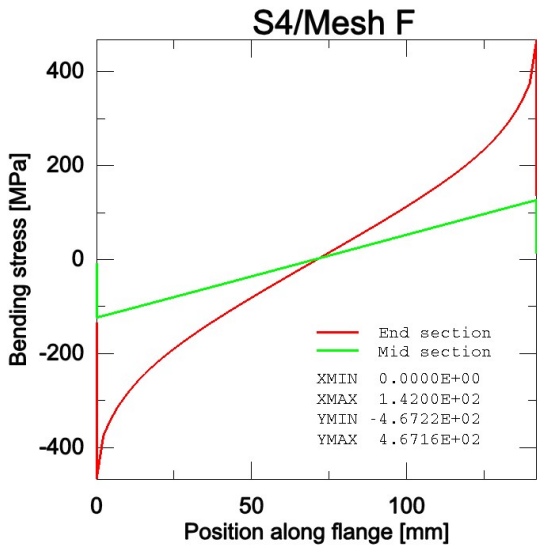
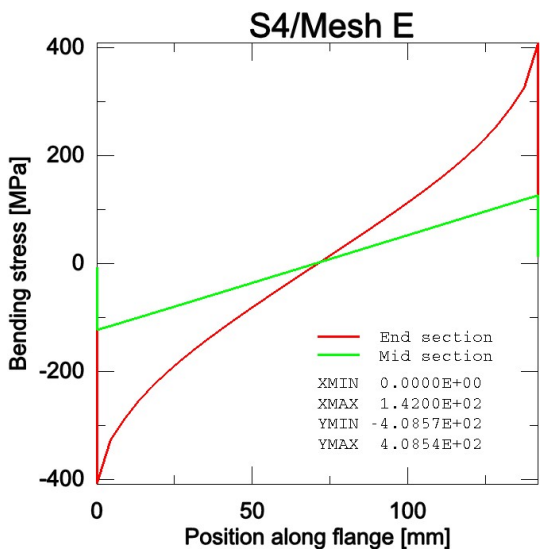
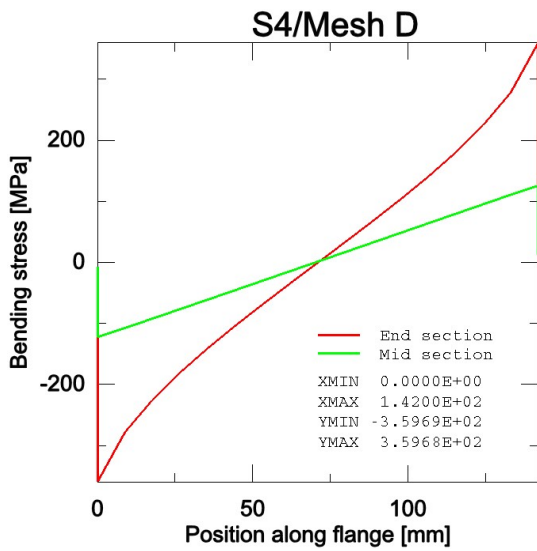
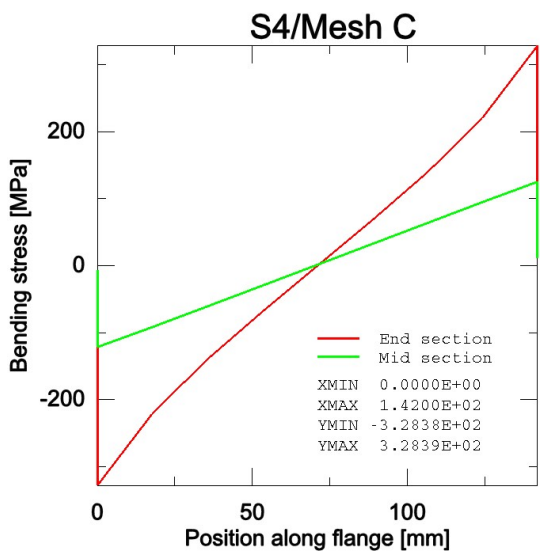
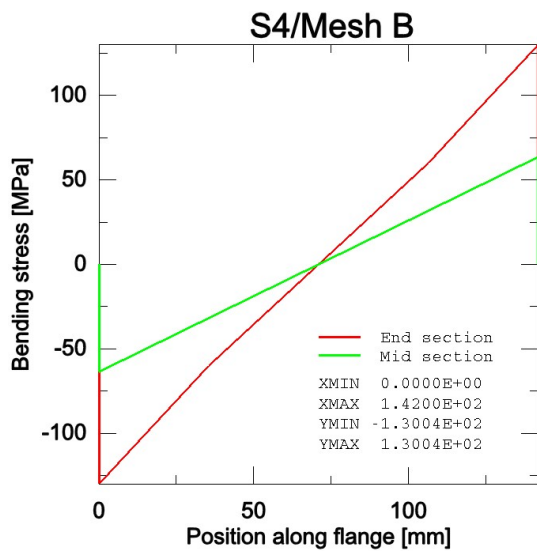
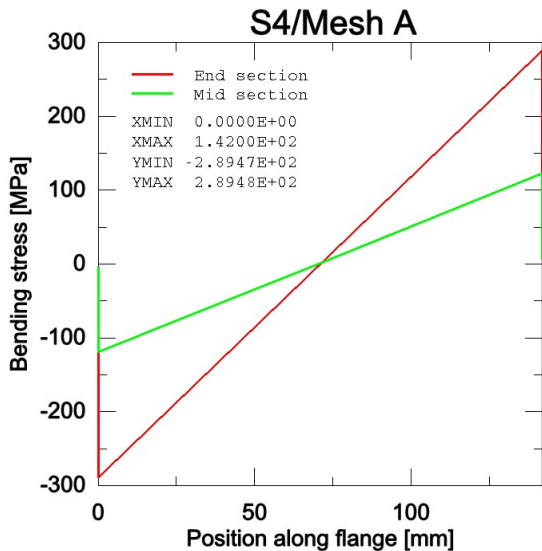


Figure 8: Bending stresses over the height of the web (the plots say “position along flange, but it should be “web”). ($z = 0$ og $z = \ell/2$ in Figure 1).

Task b) Determine the cross-section properties for the thin-walled section and performed a finite element analysis with one-dimensional beam elements compare with the results obtained in a). What is the cause of the large difference in both stresses and displacements between the two solution methods?

Note: The solution proposal is quite extensive. However, it does contain important discussions about beam elements.

Solution:

Cross-sectional constants

For beam elements, we must first determine the cross-section properties, i.e., the axial, bending, torsion, shear, and warping stiffness. To calculate warping stiffness, the location of the cross-section's shear center, C_s , has to be known.

Axial stiffness: EA

Bending stiffness: EI

Torsional stiffness: GI_T

Shear stiffness: GA/κ

Warping stiffness: EI_ω

$$A = \int_A dA = A_w + A_f = 2\tilde{b}t_w + \tilde{h}t_f = 2 \cdot 47.5 \cdot 8 + 142 \cdot 5 = 1470 \text{ mm}^2$$

$$\begin{aligned} I &= \int_A y^2 dA = \frac{1}{12} \left[2\tilde{b}t_w^3 + t_f \tilde{h}^3 \right] + 2\tilde{b}t_w \left(\frac{\tilde{h}}{2} \right)^2 \\ &= \frac{1}{12} \left[2 \cdot 47.5 \cdot 8^3 + 5 \cdot 142^3 \right] + 2 \cdot 47.5 \cdot 8 \cdot 71^2 = 5.0283 \cdot 10^6 \text{ mm}^4 \end{aligned}$$

$$I_T = \frac{1}{3} \left[2\tilde{b}t_w^3 + \tilde{h}t_f^3 \right] = \frac{1}{3} \left[2 \cdot 47.5 \cdot 8^3 + 142 \cdot 5^3 \right] = 2.2130 \cdot 10^4 \text{ mm}^4$$

$$\kappa = A / A_f = 1470 / 710 = 2.0704$$

$$e = \frac{3t_w \tilde{b}^2}{\tilde{h}t_f + 6\tilde{b}t_w} = \frac{3 \cdot 8 \cdot 47.5^2}{142 \cdot 5 + 6 \cdot 47.5 \cdot 8} = 18.11 \text{ mm}$$

$$\begin{aligned} I_\omega &= \int_A \omega^2 dA = \frac{2}{3} \left(\frac{\tilde{h}}{2} \right)^2 \left\{ e^2 \left(\frac{\tilde{h}}{2} \right) t_f + \left[e^3 + (\tilde{b} - e)^3 \right] t_w \right\} \\ &= \frac{2}{3} \cdot 71^2 \left\{ 18.11^2 \cdot 71 \cdot 5 + \left[18.11^3 + (47.5 - 18.11)^3 \right] \cdot 8 \right\} \\ &= 1.2335 \cdot 10^9 \text{ mm}^6 \end{aligned}$$

Finite element analysis with beam elements

When a cantilever beam is modeled with one-dimensional beam elements, the challenge consists of choosing the right type of element and appropriate cross-sectional profile. The choice is then between "*Arbitrary*" or "*generalized*". In our case, it is most appropriate to select "*Arbitrary*", which involves specifying location and thickness of the segments that define the cross-section. This is in principle very similar to what is done when the location of the middle plane of the shells are specified, when the cross-section is modeled with shell elements. Using "*Arbitrary*" the program calculates all required cross-section constants based on the cross-section located in relation to the local axis system selected. If one chooses to use "*Generalized*", all cross-sectional constants must be calculated and specified explicitly by the user. In our case, we have all the necessary cross-sectional measures available, provided that the location of the longitudinal axis coincides with the cross-section's center of gravity. Nevertheless, we have chosen profile type "*Arbitrary*". The background for this is that we later decide to move the cross-section local axis system so that it coincides with the shear center C_s .

In ABAQUS one can choose between elements based on *Euler-Bernoulli* and *Timoshenko* beam theory. Euler-Bernoulli is often referred to as elementary beam theory, assumes that the deformation occurs according to *Navier's hypothesis*; plane cross-sections that are normal to the beam axis remain plane and normal to the beam axis after bending. In ABAQUS is Euler-Bernoulli beam elements (B23 and B33) based on cubic interpolation polynomials of both axial and transverse displacements. B23 and B33 are C^1 –elements, that in addition to bending with regards to the beam's two main axis also describe twisting or torsion.

Beam elements based on Timoshenko beam theory (B21, B22, B31 and B32) are C^0 – elements, that in addition to bending of the two main axes also describe torsion and transverse shear strains for both «thin» and «thick» beams. The C^0 – elements in ABAQUS are available as both 2-node linear (B21 and B31) and 3-node quadratic (B22 and B32) elements. All Timoshenko elements in ABAQUS are formulated with reduced integration, 1-point for linear and 2-point Gauss integration for the quadratic element. This is done to avoid issues with shear locking.

As opposed to the C^1 –elements that only can describe small strains the C^0 –elements are formulated to describe large membrane (axial) and bending strains, while transverse and torsional strains are assumed to be moderate («small»). Even if C^0 – elements are more general than the C^1 –elements, the C^1 –elements are much better suited for slim beam structures where the shear deformations are of lesser importance. It is for such cases much more accurate, and a higher convergence rate especially in terms of displacements, $e_u = O(h^{p+1})$, while for strains/ stresses, $e_\varepsilon = e_\sigma = O(h^{p+1-m}) \Rightarrow e_\sigma^{EB} = O(h^2)$, $e_\sigma^{T1} = O(h^1)$ og $e_\sigma^{T2} = O(h^2)$, where e_σ^{EB} express the convergence rate for Euler-Bernoulli elements, while e_σ^{T1} and e_σ^{T2} express the convergence rate for linear and quadratic Timoshenko elements respectively.

For thin-walled open cross-section, composed of thin segments it may occur warping of the cross-section. If warping is restricted at the fixed end, there will be axial stresses in the flanges due to bending of the flanges in their own plane. The C^0 – elements B31OS and B32OS in ABAQUS are linear and quadratic 3D beam elements for modeling of "Open Section". The formulation requires that warping deformation is small compared with the other strains.

Element type	Dimension	Beam - theory	Beam type	Interpolation order (p)						Strains				
				u	v	w	θ_x	θ_y	θ_z	ε_m	ε_b	ϕ	γ	ω
B23	2D	EB	C^1	3	3	3	2	2	1	S	S	S	-	-
B21	2D	T	C^0	1	1	1	1	1	1	L	L	S	S	-
B22	2D	T	C^0	2	2	2	2	2	2	L	L	S	S	-
B33	3D	EB	C^1	3	3	3	2	2	1	S	S	S	-	-
B31	3D	T	C^0	1	1	1	1	1	1	L	L	S	S	-
B32	3D	T	C^0	2	2	2	2	2	2	L	L	S	S	-
B31OS	3D	T	C^0	1	1	1	1	1	1	L	L	S	S	S
B32OS	3D	T	C^0	2	2	2	2	2	2	L	L	S	S	S

Table 2: Beam elements in ABAQUS (EB = Euler-Bernoulli, T = Timoshenko, w = axial displacements, u, v = transverse displacements, θ_z = twist about the beam axis, θ_x, θ_y = rotation about cross-section axes, ε_m = axial strains, ε_b = bending strains, ϕ = torsion deformation, γ = transverse shear strains, ω = vault deformation, S,L = small/large strains).

Element type	N_{els}	Eccentric loading		Centric loading		
		v_f^b	θ_z^b	\hat{v}^b	\hat{v}_f^b	$\hat{\theta}_z^b$
B33	1	-6.1203	-0.21077	-11.126	-6.157	-0.21077
	10	-6.1203	-0.21077	-11.126	-6.157	-0.21077
B31	1	-5.9946	-0.21077	-11.001	-6.032	-0.21077
	10	-6.1941	-0.21077	-11.200	-6.231	-0.21077
	50	-6.1961	-0.21077	-11.202	-6.233	-0.21077
	100	-6.1961	-0.21077	-11.202	-6.233	-0.21077
B32	1	-6.1962	-0.21077	-11.202	-6.233	-0.21077
	10	-6.1961	-0.21077	-11.202	-6.233	-0.21077
B31OS	1	-4.4100	-0.12271	-7.3245	-4.417	-0.12271
	10	-4.6160	-0.12307	-7.5388	-4.623	-0.12307
	50	-4.6185	-0.12310	-7.5421	-4.626	-0.12310
	100	-4.6186	-0.12310	-7.5422	-4.627	-0.12310
B32OS	1	-4.6270	-0.12356	-7.5616	-4.635	-0.12356
	10	-4.6186	-0.12310	-7.5422	-4.627	-0.12310
	50	-4.6186	-0.12310	-7.5422	-4.627	-0.12310

Table 3: Vertical displacement and rotation of length axis for different choices of axis system.

Table 3 shows the results obtained respectively B33, B31, B32, B31OS and B32OS for different element divisions and different choices of local axis system. The element analysis was first run with local axis system located in the center of gravity of the web, as shown in Figure 1. The load acts eccentric with respect to the local axis system, which requires that it must be applied as a concentrated point load, P, and a concentrated torque M, at the end of cantilever beam:

$$P = -\tilde{q}_o \tilde{b} = -1.0 \cdot 10^4 \text{ N}$$

$$M = -\frac{P\tilde{b}}{2} = -2.375 \cdot 10^5 \text{ Nmm}$$

The offsets in columns 3 and 4 of Table 3 refers to when the load acts eccentrically. Accordingly, these values represent the displacement of the center of gravity of the web. In turn, the local axis system moved, as shown in Figure 9, so that the resultant of the load acts centric with respect to the local axis system $(\hat{x}, \hat{y}, \hat{z})$. The offsets in column 5 and 7 in Table 3 refers to the same local axis system. Column 6 in Table 3 represents the vertical displacement of the web's center, which according to Figure 9 can be calculated from the vertical displacement and rotation, of the beam local axis system $(\hat{x}, \hat{y}, \hat{z})$:

$$\hat{v}_f^b = \hat{v}^b - \frac{\tilde{b}}{2} \cdot \sin \hat{\theta}_z^b$$

As expected, the Euler-Bernoulli elements and the quadratic Timoshenko elements converge very fast compared to the linear Timoshenko elements. B31, B32 and B33 elements are based on *Saint-Venant torsion theory*, and thus yield the same torsion deformation. If we compare vertical displacement of the web's middle point (v_f^b in Table 3) for B33 with B31/B32, it increases with about 1.2 % due to shear strains, while the influence of warping, represented by the difference between B31/B32 and B31OS/B32OS, is the critical one with respect to both vertical displacement, v_f^b , and rotation, θ_z^b .

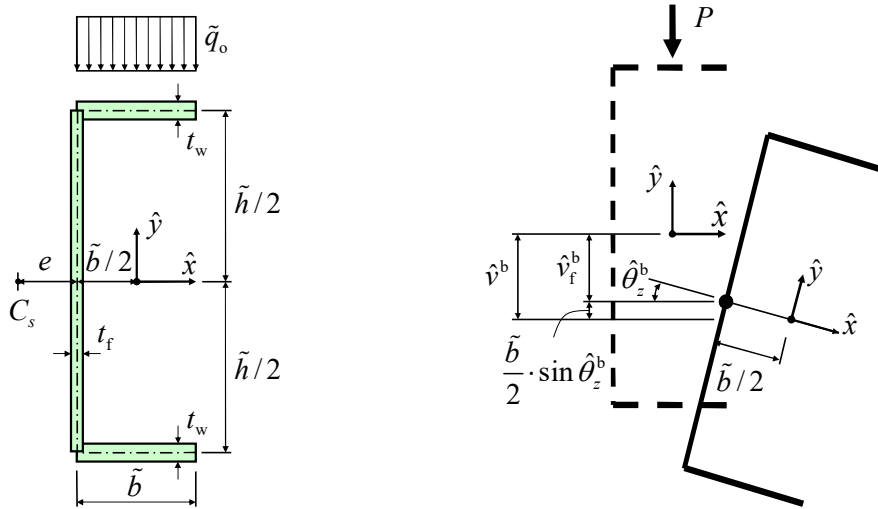


Figure 9: Beam's local axis system with centric load application before and after deformation.

If we compare the displacement of the free end from the shell analysis, v_f^s, θ_z^s , with beam analysis using B32OS, v_f^b, θ_z^b , the differences are larger:

Shell model (S4 element): $v_f^s = -4.32 \text{ mm}, \theta_z^s = -\cos^{-1}(9.23 + 9.23/142) = -0.130$
 Beam model (B32OS): $v_f^b = -4.62 \text{ mm}, \theta_z^b = -0.123$

Displacement with beam model using element B32OS yields 7 % larger deflection and 5 % less rotation of the free end compared to a refined shell model.

Beam analyzes using the finite element B32OS gives the following stresses at ($z = \ell/2$):

$$\begin{aligned} V_y^b &= -1.0 \cdot 10^4 \text{ N} & \Rightarrow \tau_s^{b,\max} &= \kappa \frac{3V_y^b}{2A} = -10.56 \text{ MPa} \\ M_x^b &= 4.5 \cdot 10^6 \text{ Nmm} & \Rightarrow \sigma_b^{b,\max} &= \frac{M_x^b}{I} \cdot \frac{\tilde{h}}{2} = 63.54 \text{ MPa} \\ M_z^b &= -4.186 \cdot 10^5 \text{ Nmm} & \Rightarrow \tau_{\text{stv}}^{b,\max} &= \left| \frac{M_z^b}{I_T} \cdot t_w \right| = 151.3 \text{ MPa} \\ B^b &= -1.567 \cdot 10^8 \text{ Nmm}^3 & \Rightarrow \sigma_{\text{wpp}}^{b,\max} &= \frac{B^b}{I_\omega} \cdot \omega = 74.33 \text{ MPa} \end{aligned}$$

Figure 10 shows how both the bending moment, M_x^b , bi-moment, B^b , and resulting axial stress distribution at the cantilevers middle section ($z = \ell/2$).

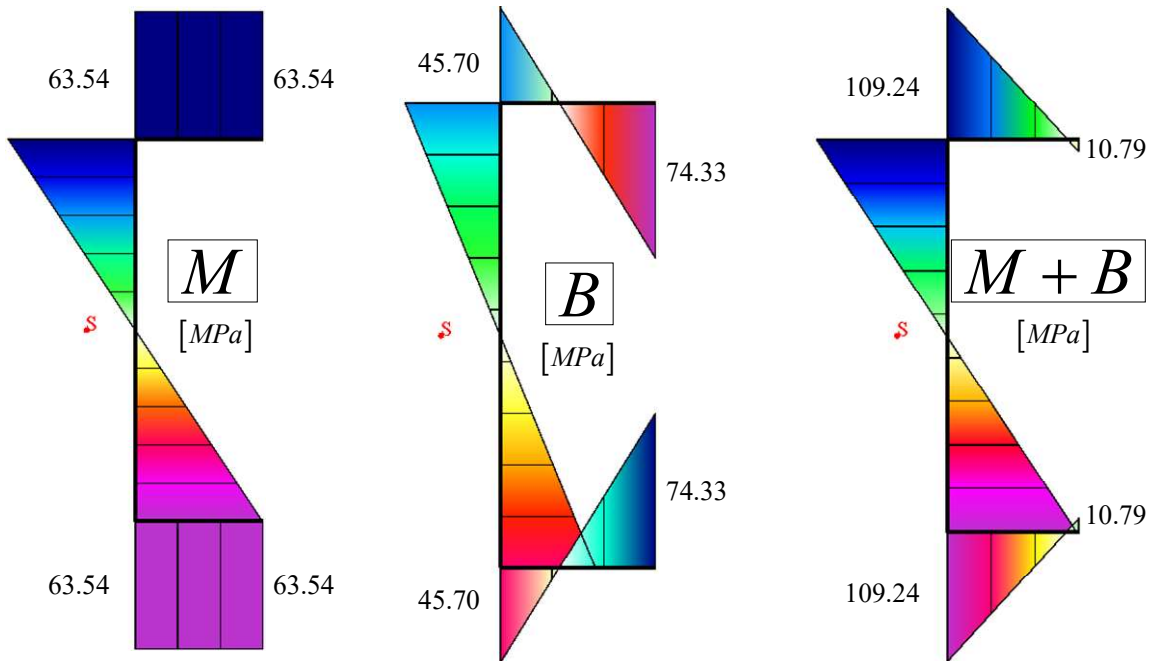


Figure 10: Distribution of axial stresses for middle section ($z = \ell/2$).

If we compare the maximum axial stresses at the middle section, $\sigma^{b,\max} = 109 \text{ MPa}$, with the corresponding shell element solution, $\sigma^{s,\max} = 125 \text{ MPa}$, the beam element model yields 12 % less axial stress compared to a refined shell model (using S4 elements).

The cause of the deviation that is relatively small in terms of displacements and somewhat larger for axial stresses is that the beam model in ABAQUS does not sufficiently account for the warping effect. In addition, there are also local bending in the shell model when the load is applied to the top of the flange that is not captured by the beam model.

Task c) Perform hand calculations based on elementary beam theory where only bending deformations are considered.

Solution:

Analytical beam solutions

As a control, the results of the FEA could be compared to analytical beam solutions. We start by looking at the deflection of the free end with respect to elementary beam theory.

Using the principle of virtual displacements, one could calculate the contributions from bending and transverse shear:

$$\begin{aligned} v^{\text{eb}} &= \int_{\ell} \frac{M^0 M^1}{EI} dz + \int_{\ell} \kappa \frac{Q^0 Q^1}{GA} dz = \frac{q_0 b \ell^3}{3EI} + \kappa \frac{q_0 b \ell}{GA} \\ &= \frac{200 \cdot 50 \cdot 900^3}{3 \cdot 2.1 \cdot 10^5 \cdot 5.0283 \cdot 10^6} + 2.0704 \cdot \frac{200 \cdot 50 \cdot 900}{8.0769 \cdot 10^4 \cdot 1470} = 2.458 \text{ mm} \end{aligned}$$

Based on *Saint-Venant torsion theory* (plane cross-sections deform without strains in its own plane such that they all obtain the same curved shape) The torsion angle is given by the formula:

$$\theta_z^{\text{stv}} = \frac{M_T \ell}{GI_T} = \frac{q_0 b (e + \tilde{b}/2) \ell}{GI_T} = \frac{200 \cdot 50 \cdot (18.11 + 47.5/2) \cdot 900}{8.0769 \cdot 10^4 \cdot 2.213 \cdot 10^4} = 0.21077$$

Saint-Venant torsion theory is based on unrestricted warping \Rightarrow displacement w in the beam's axial direction, z , is unrestricted. However, if the cross-section is restricted against warping it will build up axial stresses. These axial stresses are the cause of the *bi-moment*. We note that the bi-moment stress neither leads to resultant axial force, bending moment or shear forces.

To find the bi-moment, we can apply Vlasov-theory. This is outside the curriculum for this course. For this problem, we will see that by considering that the cross-section is restricted against warping, we reduce the torsion angle significantly.

Vlasov-theory for torsion and bending express the resulting axial stress on the form:

$$\sigma_z = \frac{N}{A} - \frac{M_x}{I_x} y - \frac{M_y}{I_y} x - \frac{B}{I_\omega} \omega$$

where ω is the sector coordinate, and the warping parameter, I_ω express the quadratic warping area moment, and B express the bi-moment:

$$\begin{aligned} \omega &= \int d\omega \\ I_\omega &= \int_A \omega^2 dA \end{aligned}$$

$$B = EI_{\omega} \frac{d^2\theta_z}{dz^2} = EI_{\omega}\theta_z''$$

Based on equilibrium considerations of a thin-walled beam subjected to torsion, one can establish a strong form for the torsion problem with a third order differential equation:

$$EI_{\omega}\theta_z''' - GI_T\theta_z' = -M_T$$

With a general solution:

$$\theta_z = C_1 + C_2 e^{kz} + C_3 e^{-kz} + \frac{M_T}{GI_T} z \quad \text{where} \quad k = \sqrt{\frac{GI_T}{EI_{\omega}}}$$

For a cantilevered beam which is restricted in terms of warping in one end and free in the other, the boundary conditions for the torsion problem are given by:

$$\text{Fixed end } (z = 0): \theta_z = \theta_z' = 0$$

$$\text{Free end } (z = \ell): \sigma_x = -\frac{B}{I_{\omega}} \omega = 0 \Rightarrow B = EI_{\omega}\theta_z'' = 0 \Rightarrow \theta_z'' = 0$$

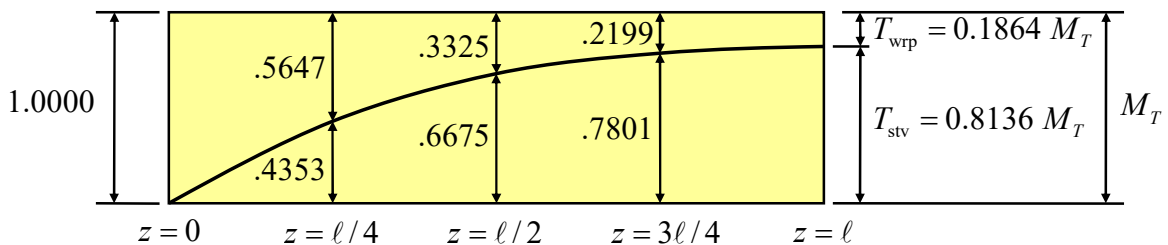
The three constants can then be determined and the expression for the torsion angle θ_z , Saint-Venants torsion moment, T_{stv} , and bi-moment, B , according to Vlasov-theory is presented as:

$$\begin{aligned} \theta_z &= \frac{M_T \ell}{GI_T} \left\{ \frac{z}{\ell} - \frac{1}{k\ell(e^{k\ell} + e^{-k\ell})} [e^{k\ell}(1 - e^{-kz}) - e^{-k\ell}(1 - e^{kz})] \right\} \\ T_{\text{stv}} &= GI_T \theta_z' = M_T \left[1 - \frac{e^{k\ell} e^{-kz} + e^{-k\ell} e^{kz}}{e^{k\ell} + e^{-k\ell}} \right] \\ B &= EI_{\omega}\theta_z'' = \frac{M_T}{k} \cdot \frac{e^{k\ell} e^{-kz} - e^{-k\ell} e^{kz}}{e^{k\ell} + e^{-k\ell}} \end{aligned}$$

Warping torsion moment T_{wrp} that is caused by the cross-section being restricted against warping is given as:

$$M_T = T_{\text{stv}} + T_{\text{wrp}} \Rightarrow T_{\text{wrp}} = M_T - T_{\text{stv}}$$

Figure 11 shows how torsion moment, M_T , is distributed between Saint-Venant torsion and warping torsion along the beam where the torsion angle, θ_z , and bi-moment, B , varies along the beam axis.



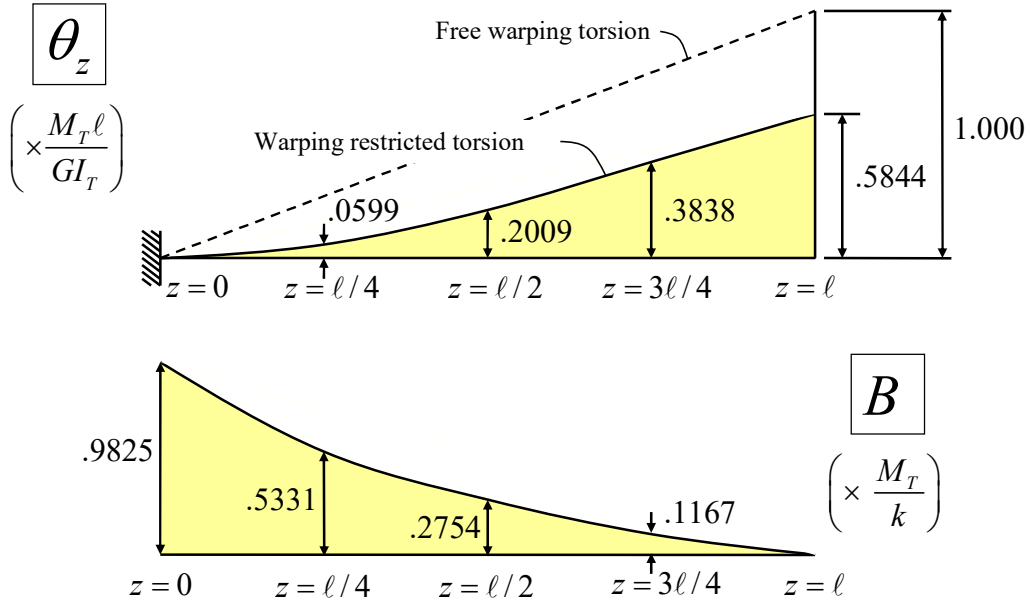


Figure 11: Distribution of torsion moment and angle and bi-moment in length direction.

It is clearly demonstrated in Figure 11 that by taking into account that the cross-section is restricted against warping the torsion angle is drastically reduced.

$$\theta_z^{\text{vsv}} = 0.5844 \frac{M_T \ell}{G I_T} = 0.1232$$

Vertical displacement with regards to elementary beam theory, v_s^{eb} , is referred to the cross-section's shear center, C_s . Vertical displacement in the mass center of the web has to be calculated according to the geometric consideration seen in Figure 9:

$$v_f^{\text{vsv}} = v^{\text{eb}} + e \cdot \sin \theta_z^{\text{vsv}} = 2.458 + 18.11 \cdot \sin(0.1232) = 4.683 \text{ mm}$$

Task d) Compare the results obtained in a), b) and c), and explain the observed differences.

Solution:

If we compare the displacement of the free end in terms of the shell element solution, v_f^s, θ_z^s , and in terms of the beam solution with the B32OS element, v_f^b, θ_z^b , with the analytical solution according to Vlasov-theory, $v_f^{\text{vsv}}, \theta_z^{\text{vsv}}$, we see that the differences are rather small:

Shell model (S4):	$v_f^s = -4.32 \text{ mm}, \theta_z^s = -0.130$
Beam model (BS32OS):	$v_f^b = -4.62 \text{ mm}, \theta_z^b = -0.123$
Vlasov-theory:	$v_f^{\text{vsv}} = -4.68 \text{ mm}, \theta_z^{\text{vsv}} = -0.123$

Displacements in terms of Vlasov-theory yields 8 % larger deflection and 5 % less rotation of the free end compared to a refined shell model. Similarly, Vlasov-theory yield 1 % larger deflection, but the same end rotation as the beam model (B32OS).

If we compare the stress resultants in the cantilever's middle section calculated with Vlasov-theory with results using beam element B32OS, it is obviously no difference in the shear force, V_y^b , and bending moment, M_x^b , while the bi-moment according to Vlasov-theory, B^{vsv} (see Figure 11), is 0.3 % less than that what is seen in the beam element analysis with the BS32OS element, B^b :

$$\text{Vlasov-theory: } B^{vsv} = 0.2754 \cdot \frac{M_T}{k} = 0.2754 \cdot \frac{-4.186 \cdot 10^5}{2.627 \cdot 10^{-3}} = -4.388 \cdot 10^7 \text{ Nmm}^3$$

$$\text{Beam model (BS32OS): } B^b = -4.4033 \cdot 10^7 \text{ Nmm}^3$$

The contribution of the bi-moment to the resulting axial stress is thus reduced, such that the resulting axial stress according to Vlasov-theory in the beam's center section, $\sigma^{vsv,\max} = 109 \text{ MPa}$, is roughly 12 % lower than the solution, $\sigma^{s,\max} = 125 \text{ MPa}$, for a refined shell model with S4 elements.

As mentioned above, the explanation to why the results are so different between the three models is that we have combined bending and torsion, as well as local deformations due to the load being applied at the top of the flange which cannot be modelled by a beam model.

Task e) Suggest measures to perform finite element analyses with shell elements such that they can be comparable to the results with beam elements.

Solution:

Shell model with load applied in the cross-section's shear center

If the load is applied in the cross-section's shear center, C_s , it is expected that both the shell and beam analysis should yield the same results as elementary beam theory corrected for shear deformations.

To ensure that the load is properly transferred to the cantilevered beam the point of load application, C_s , must be kinematically coupled to the end section of the beam. In ABAQUS this can be done by selecting the following options in the dialog box for “**Create Constraint**”:

Constraint Type → Coupling
Coupling Type → Kinematic

A kinematic coupling is a surface-based coupling, where the movement of all nodes on that surface is directly related to the movement of a reference node. The reference node for our particular case is a node placed in the shear center, C_s , which is then coupled to the end surface of the cantilevered beam. This means that all degrees of freedom that are included in the coupling will move along with the shear center. By specifying a kinematic coupling of all six degrees of freedom between the end surface and the shear center it will act as a rigid link. Which in turn means that the rotation of the end surface follows the rotation of the shear center.

Figure 12 shows a convergence plot of the vertical displacement of the free end for all 28 combinations of element and mesh that has been analyzed when the load is applied in the shear

center, C_s . The displacement in Figure 12 is registered in the middle of the web. The convergence plots show that the linear triangular elements STRI3 and S3 converge significantly slower than the rest of the elements S4, S8R and STRI65. All elements do however seem to converge towards the same solution:

$$v_f^{s,C_s} = 2.466 \text{ mm}$$

This is practically equal to the elementary beam theory solution corrected for shear deformations, $v^{eb} = 2.458 \text{ mm}$.

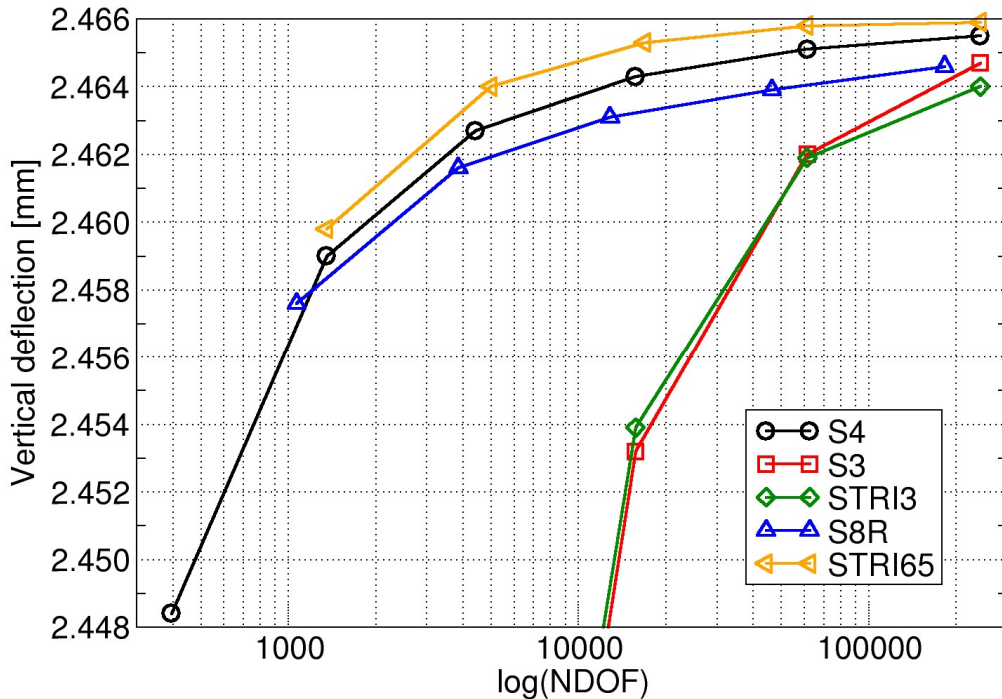


Figure 12: Convergence of deflection of free end with load applied in C_s .

Figure 13 shows a similar convergence plot of maximum bending stress in the fixed end. Similarly, with what was observed when the load was applied to the top flange it seems like none of the elements are converging. Which is caused by the stress concentrations at the top and bottom of the web in the fixed end. To avoid these stress concentrations, we again consider a cross-section that is not influenced by the boundary effects.

Figure 14 shows the convergence of maximum bending stresses for $z = \ell/2 = 450 \text{ mm}$. As mentioned already, the linear triangular elements S3 and STRI3 cannot describe a linear variation of stresses/strains within the element. This in turn explains why the convergence is much slower with those elements compared to the rest. As is evident from Figure 14b, which shows an enlarged view of the convergence plot, the remaining elements S4, S8R and STRI65 all converge towards the same value:

$$\sigma^{s,\max} = 63.57 \text{ MPa}$$

Which is equal to the beam theory solution, $\sigma^{b,\max} = \frac{M_x^b}{I} \cdot \frac{\tilde{h}}{2} = 63.54 \text{ MPa}$.

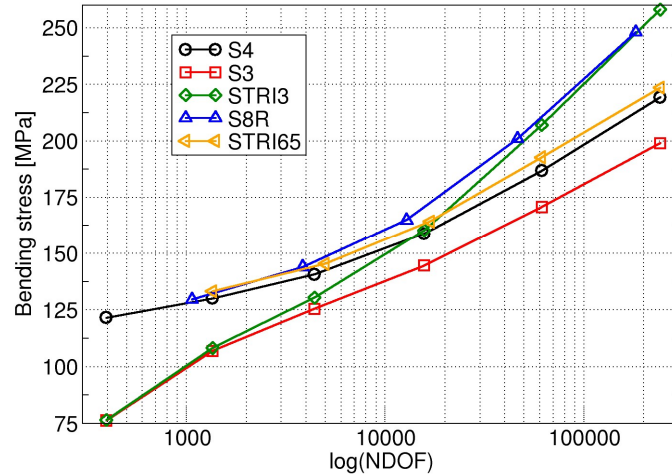
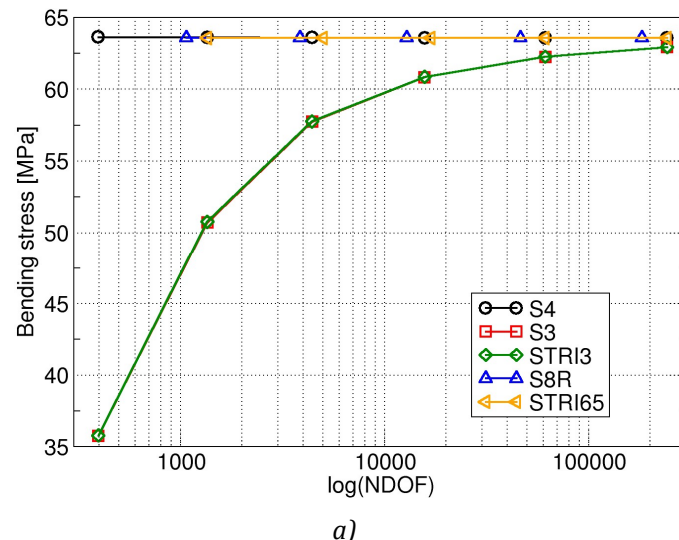
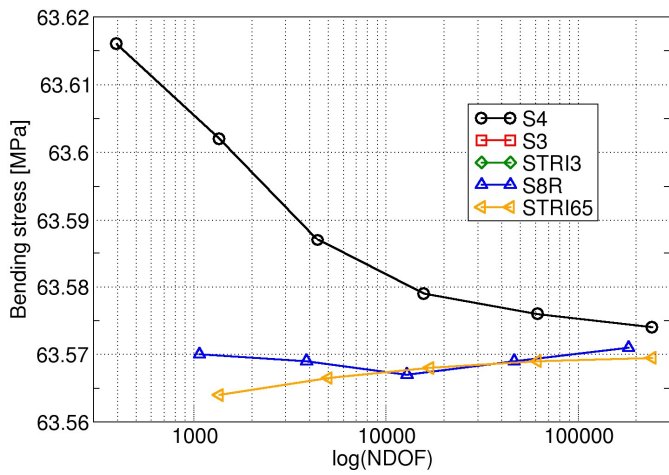


Figure 13: Convergence of maximum bending stress at the fixed end with the load in C_s .



a)



b)

Figure 14: Convergence of maximum bending stress at the beam's mid-section with load in C_s .

Beam model with load applied in the shear center

Local axis system is moved to the shear center, C_s , such that the beam axis coincide with the shear center and apply the load, P , centric with respect to the local axis system.

Table 4 shows vertical displacement of the shear center achieved with B33, B31, B32, B31OS and B32OS respectively for different meshes. As expected, the Euler-Bernoulli and the quadratic Timoshenko elements converge very fast compared to the linear Timoshenko elements. A single cubic Euler-Bernoulli element or quadratic Timoshenko element yields the same accuracy as 50 linear Timoshenko elements. All five elements yield zero torsional deformation ($\theta_z^{b,C_s} \cong 0$) as expected. The Euler-Bernoulli beam, B33, also give the same results as the bending part of elementary beam theory as expected:

$$v_b^{\text{eb}} = \int_{\ell} \frac{M^0 M^1}{EI} dz = \frac{q_0 b \ell^3}{3EI} = \frac{200 \cdot 50 \cdot 900^3}{3 \cdot 2.1 \cdot 10^5 \cdot 5.0283 \cdot 10^6} = 2.301 \text{ mm}$$

However, we should note that the shear contribution for all the Timoshenko beams is too small. It deviates with a factor equal to the shear factor κ from elementary beam theory corrected for shear deformations $v^{\text{eb}} = 2.458$ mm. This indicates that the Timoshenko elements B31, B32, B31OS and B32OS, does not correct for the shear deformations with the factor κ . Similar deviations are present for deflection for the analysis with the load applied to the top of the flange.

The calculated stress resultants, V_y^{b,C_s} and M_x^{b,C_s} , are however coincident with elementary beam theory.

Element Type	N_{els}	v^{b,C_s}
B33	1	-2.3031
	10	-2.3031
B31	1	-2.1774
	10	-2.3769
	50	-2.3789
	100	-2.3789
B32	1	-2.3790
	10	-2.3789
B31OS	1	-2.2014
	10	-2.4009
	50	-2.4029
	100	-2.4029
B32OS	1	-2.4030
	10	-2.4030

Table 4: Vertical displacement of the beam axis with load applied in the shear center, C_s .

A note on how finite element field quantities are determined.

Element-based field quantities, like stress resultants, are calculated in the element integration points and extrapolated to the element nodes. Extrapolated values are generally less accurate than the values sampled in the integration points. This means that one must use a relatively large number of elements to achieve accurate results in areas with large gradients. To illustrate this further, we will look at the stress resultants calculated in the element B32OS when the model consists of only one element (N_{els}). We look back at the problem when the load acts eccentric with regards to the local axis system, and is subjected to a point load, P , and a concentrated moment, M , at the end of the cantilevered beam.

B32OS is a quadratic element with two integration points (Gauss points), which means that all element-based field quantities are sampled in these two points and then extrapolated to the nodes. For our case the shear force, V_y , is constant along the whole length of the beam, while the bending moment, M_x , vary linearly. A linear interpolation would then yield correct values in the beam direction. The bi-moment, B , varies exponentially as shown in Figure 11. Such that even if the extreme values of the displacements, v^b and θ_z^b , and the stress resultants, V_y^b and M_x^b are accurately modelled with only one element, we see from Figure 15 that this is not the case for the bi-moment, B^b . The red line shows how the bi-moment varies in the length direction with then element (B32OS). Even if B^b is coinciding with the Vlasov-theory solution in the integration points, the linear extrapolation to the nodes yields too low values. The deviation is at 16 % in the fixed end. The solution to this problem is to reduce the element size close to the fixed end.

Please note that you must prescribe the warping degree of freedom θ'_z equal to zero in the fixed end, if not the cross-section will not be restricted with respect to warping. ABAQUS/CAE does not allow you to prescribe values of θ'_z , as it occurs as the seventh degree of freedom for all nodes linked to elements of type B31OS or B32OS. This can be solved by specifying this boundary condition in the input file:

```
*Boundary
End-node, 1, 7
```

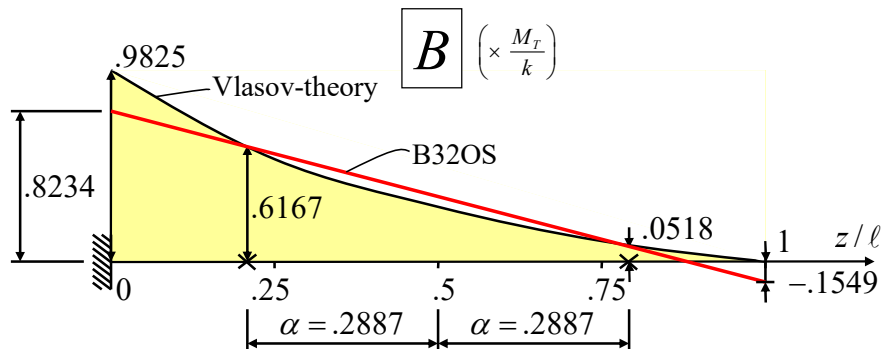


Figure 14: Distribution of the bi-moment in the length direction.

Conclusions from the comparisons

Shell model:

Use elements that can describe linear variation of strain in the plane of the element. Element S4, which is a 4-node rectangular element, converges quickly and provides results as precise as higher order triangular and square elements S8R and STRI65, for similar number of degrees of freedom. The linear triangular elements S3 and STRI3 converges significantly worse than the other elements that have been tested and is not recommended when the model is bending in the plane of the elements.

Beam model:

For open thin-walled cross-sections, it is recommended to use the quadratic Timoshenko element B32OS. The element converges quickly and yield accuracy similar to that of analytical solutions according to Vlasov-theory. It should be noted that if the warping degree of freedom θ_z' is not prescribed properly the cross-section will not be restricted in terms of warping deformations. Users of ABAQUS/CAE should be careful to ensure that these boundary conditions are correctly applied in the input file when using elements B32OS (and B31OS) as mentioned earlier.

Choice of model:

If one is not careful to conduct proper selection of beam elements, including prescribing the appropriate degrees of freedom, one should base the analysis on a shell model with S4 elements with a minimum of 8 elements over the height of the web (Mesh C). To account for local deformations in the region where the load is applied one has to use a shell model (or a solid model). The conducted study shows that a beam model with B32OS elements give an accuracy of displacements that are comparable with the shell model. The shell model does however yield 12% higher values on the maximum normal stresses.

Task f) What will be the consequences of allowing for non-linear geometry in the finite element solution. Hint: You can allow for non-linear geometry by opening the **Step Manager**, then **Edit step** and change **Nlgeom** from **Off** to **On**.

Solution:

By re-running one of the models using Nlgeom, we see that applying non-linear geometry effects does affect our problem somewhat for the specified load. We can for example look at the model with S4 elements with size 30 mm. The U1 displacement in the linear model seems to be symmetric about the YZ-axis, while it is non-symmetric for the non-linear model. *Non-linear effects in finite element methods effects will be studied further in the course TKT4197.*

Model (S4 with 30 mm elements)	U1 (min/max) [mm]	U2 (min/max) [mm]	U3 (min/max) [mm]	S11 (min/max) [MPa]
Linear geometry effects	-9.19 / 9.19	-12.21 / 0.00	-0.54 / 0.54	-354.9 / 247.9
Non-linear geometry effects	-12.87 / 4.36	-12.18 / 0.00	-0.69 / 0.44	-366.6 / 250.5

Table 5: Results from a linear model and a non-linear model of the beam with S4 elements.

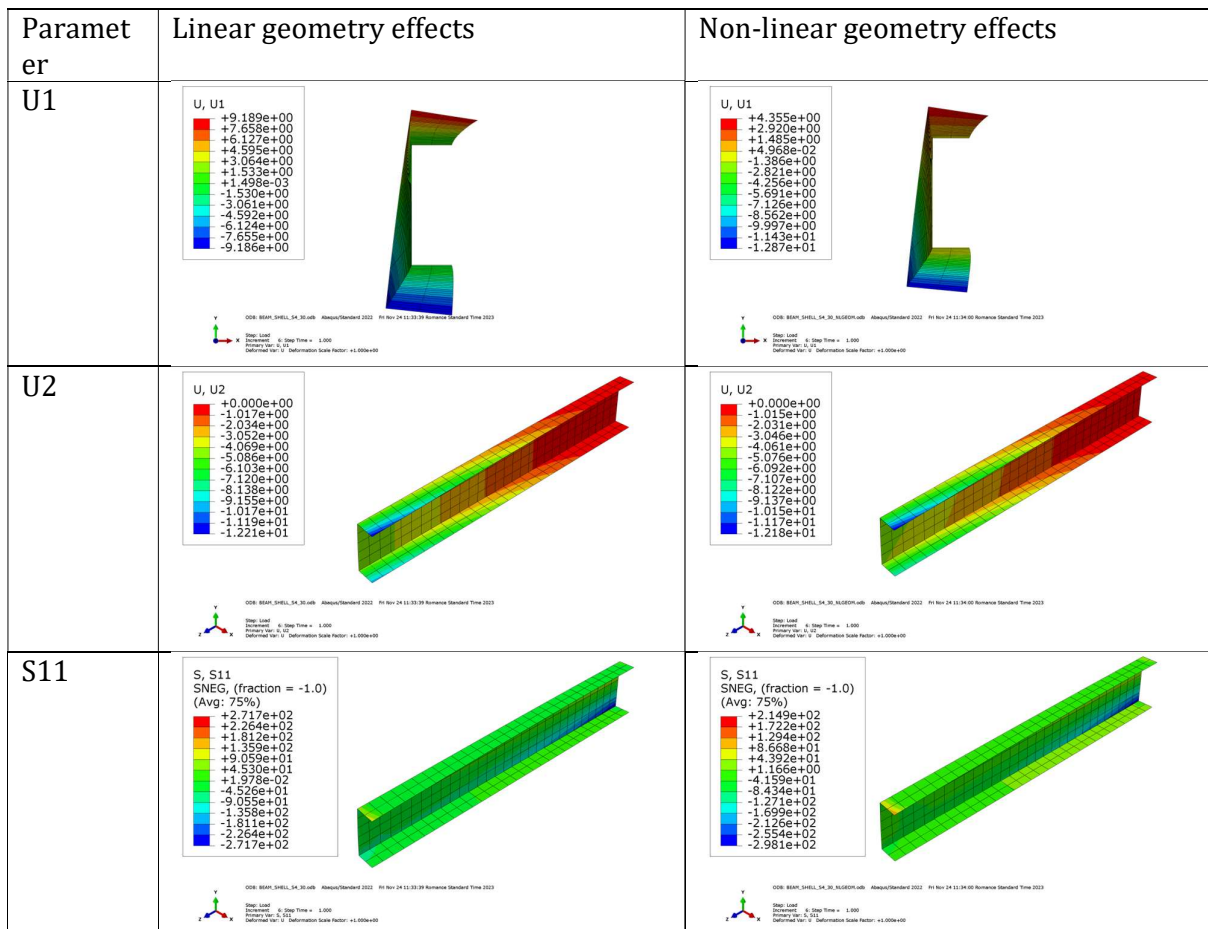


Table 6: Contour plots from a linear model and a non-linear model of the beam with S4 elements.